JOURNAL OF Materials CHEMISTRY

Synthesis and crystal structure of $K_2Sr_{1.5}Ta_3O_{10}$ and $K_2Sr_{1.5}Ta_3O_{10}\cdot H_2O$: two new layered perovskite compounds

F. Le Berre, M. P. Crosnier-Lopez, Y. Laligant and J. L. Fourquet

Laboratoire des Fluorures (UMR 6010, CNRS) Faculté des Sciences et Techniques du Mans, Université du Maine, Avenue O. Messiaen, 72085 Le Mans Cedex 9, France

Received 4th July 2001, Accepted 25th October 2001
First published as an Advance Article on the web 4th January 2002

We present a full structural characterisation by powder diffraction of $K_2Sr_{1.5}Ta_3O_{10}$ and $K_2Sr_{1.5}Ta_3O_{10}\cdot H_2O$, the structures of which are related to that of the Ruddlesden–Popper $n = 3$ member layered perovskite phases ($K_2Sr_{1.5}Ta_3O_{10}$, *I*4/*mmm*, $a = 3.9626(1)$ Å, $c = 30.3257(7)$ Å, $Z = 2$; $K_2Sr_{1.5}Ta_3O_{10}\cdot H_2O$, *P*4/*mmm*, $a = 3.9499(2)$ Å, $c = 17.031(3)$ Å, $Z = 1$). We show that $K_2Sr_{1.5}Ta_3O_{10}$ can be synthesized either directly from conventional procedures or by controlling the continuous thermal decomposition of $K_2SrTa_2O_7$ ($n = 2$ member) following the scheme: $K_2SrTa_2O_7 \rightarrow 2/3\ K_2Sr_{1.5}Ta_3O_{10} + 1/3\ K_2O$. $K_2Sr_{1.5}Ta_3O_{10}$ undergoes a fast and reversible hydration process studied by DTA/TGA experiments. In both the anhydrous and mono-hydrated phases, most of the K^+ ions are located in the interlayer between the perovskite slabs constituted by a stacking of three TaO_6 octahedra. The remainder of the K^+ ions, all the Sr^{2+} ions and vacancies are distributed on the twelve coordinated A sites of the perovskite blocks. In the case of $K_2Sr_{1.5}Ta_3O_{10}\cdot H_2O$, the water molecules are found in the interlayer on the (002) plane.

Introduction

We recently reported the synthesis and crystal structure of new oxides with general formula $Li_2A_{0.5n}B_nO_{3n+1}$ (A = Ca, Sr, B = Nb, Ta),[1,2] which belong to a family of oxides related to the layered perovskite Ruddlesden–Popper (RP) type. The latter correspond to the formulation $A'_2[A_{n-1}B_nO_{3n+1}]$ where n defines the number of BO_6 octahedra forming perovskite layers which are separated by A′ cations, A atoms occupying the 12-coordinated perovskite cages. The interaction between the slabs determines the mobility of the interlayer A′ cations; as in various RP phases this interaction is weak these compounds exhibit some interesting properties such as ion-exchange,[3] intercalation[4] and ionic conductivity.[5,6] Owing to their ion exchange capability, protonated phases $H_2A_{0.5n}B_nO_{3n+1}$ have been obtained and their dehydration process have been studied in order to rationally synthesize novel metastable 3D perovskites with exotic ordering of vacancies.[7]

Recently Ollivier and Mallouk[8] synthesized a protonated form by ion exchange of $K_2SrTa_{2-x}Nb_xO_7$ ($x = 0.0, 0.2, 0.4$) in order to prepare the metastable phases $SrTa_{2-x}Nb_xO_6$. As the structure of the starting compound $K_2SrTa_2O_7$ was not determined by Ollivier and Mallouk,[8] we decided to perform it. During this work we observed that the $n = 2$ member $K_2SrTa_2O_7$ can be transformed by heating into the $n = 3$ member $K_2Sr_{1.5}Ta_3O_{10}$ by a progressive K_2O loss. To our knowledge, this is the first example of such a transformation.

The aim of this work was to prepare new phases exhibiting high ionic conductivity. The partial occupation of the 12-coordinated perovskite cage in $K_2Sr_{1.5}Ta_3O_{10}$, is known to be an important parameter for this property and this new $n = 3$ member RP compound should be a good candidate for such a study. These results will be presented in a forthcoming paper.

We report here the synthesis and the structure determination of the $n = 3$ member $K_2Sr_{1.5}Ta_3O_{10}$ and the results concerning the hydrous form $K_2Sr_{1.5}Ta_3O_{10}\cdot H_2O$ immediately obtained in air from $K_2Sr_{1.5}Ta_3O_{10}$.

Experimental

A $K_2Sr_{1.5}Ta_3O_{10}$ sample can be synthesized by conventional solid-state reaction: the starting materials are Ta_2O_5, dried $SrCO_3$ and K_2CO_3. An excess (40%) of dried potassium carbonate was added to compensate loss due to evaporation at high temperature. The reactants were ground in an agate mortar and then pressed into pellets. The mixture was first fired in air in a platinum plate at 850 °C for 6 h with a heating rate of 10 °C min^{-1} and then at 1200 °C for 10 h. This final heating was then followed by natural cooling of the furnace. The compound was kept at 200 °C to avoid hydration.

However, better crystallized samples can be prepared by another route from the mother-phase $K_2SrTa_2O_7$ ($n = 2$ member). During our tests to synthesize a pure $K_2SrTa_2O_7$ sample, we found that new reflections appeared, their intensities increasing with temperature and time of synthesis. Referring to X-ray powder diffraction patterns of similar phases, these sharp reflections could be easily related to (00*l*) lines of a new layered compound, giving a c parameter close to 30.3 Å. Assuming the same Ta–O distances and an equivalent interlayer spacing ($\Delta z \times c$, z: coordinates of the terminal O^{2-}, close to 3.06 Å in $K_2SrTa_2O_7$), this new phase could be associated to an $n = 3$ member, corresponding then to the formulation $K_2Sr_{1.5}Ta_3O_{10}$. Such a transformation implies K_2O loss and a conservation of the Sr/Ta ratio. The process can be written in terms of eqn. (1):

$$K_2SrTa_2O_7 \rightarrow 2/3\ K_2Sr_{1.5}Ta_3O_{10} + 1/3\ K_2O \quad \text{(theoretical weight loss: 4.9\%)} \qquad (1)$$

As a measure of the completeness of transformation from $n = 2$ to $n = 3$, the experimental weight loss is close to the theoretical one: typically 5.2% weight loss was obtained for a heating of 25 min at 1400 °C for a pellet of 0.35 g. For shorter heating times, a mixture of $n = 2$ and $n = 3$ members was observed, while for longer heating times, the $n = 3$ member and the tetragonal tungsten bronze (TTB) form of $SrTa_2O_6$

 DOI: 10.1039/b105900a

were obtained. Surprisingly, according to X-ray powder diffraction (XRD) patterns the formation of higher n value phases, $n = 4$ for example, was not observed

In such a situation, it is clear that the preparation of single phase $K_2Sr_{1.5}Ta_3O_{10}$ required specific conditions due to the formation of structures with different slab thickness, as is known in the case of similar RP phases. However, to our knowledge, this is the first example where members with different n values can be synthesized starting from the same composition simply by changing the synthesis conditions. This leads consequently to an increase in A site deficiency in the higher member which leads to a 25% vacancy level in the $n = 3$ form.

The same transformation can be achieved by an extended annealing at 1050 °C, the temperature used for the synthesis of the mother-phase $K_2SrTa_2O_7$. However, such annealing implies a loss of crystallinity with a broadening of the (00l) reflection lines, which can be attributed to a disordered cationic distribution in the interlayer spacing.

It should be pointed out that whatever the synthesis route and despite our efforts, additional reflection lines corresponding to a small amount of unidentified impurity were always observed in the XRD patterns. Such a situation is often encountered in the synthesis of similar phases.[9–11]

From these results, we attempted to synthesize $Li_2Sr_{1.5}Ta_3O_{10}$ by heating at high temperature for short time the $n = 2$ form $Li_2SrTa_2O_7$. Unfortunately, we did not succeed in obtaining the $n = 3$ compound, the XRD pattern showing reflections of TTB $SrTa_2O_6$ and the $n = 2$ member.

Thermal analysis, thermogravimetric (TG) analysis coupled with differential thermal (DT) analysis, was conducted using a TA instruments SDT 2960 system with a heating rate of 5–10 °C min^{-1} under an argon flow.

For the hydrated compound, X-ray powder diffraction (XRD) patterns were recorded at room temperature using a Bruker D8 diffractometer (Cu-Kα radiation) in the 2θ range 4.2–130° (step scan: 0.02°, step time: 53 s). A hot sample holder (200 °C) was used to record the X-ray powder pattern of the anhydrous form in order to avoid hydration. XRD was recorded at 200 °C using a Siemens D500 diffractometer in the same 2θ range but with a counting time of 40 s. Structure refinement was carried out by the Rietveld method[12] using the FULLPROF profile refinement program.[13]

Results and discussion

$K_2Sr_{1.5}Ta_3O_{10}$: structural determination

Concerning the X-ray powder patterns (Fig. 1) for which conditions of collection are gathered in Table 1, the reflection positions were estimated by means of the program EVA after stripping the $K_{\alpha 2}$ component. In order to exclude all the supercells frequently encountered in such phases, auto-indexing was performed by using the program TREOR[14] applied to the first 16 detected lines for $K_2Sr_{1.5}Ta_3O_{10}$. Only one tetragonal solution was found and characterized by the conventional Figures of merit $M_{16} = 56$ and $F_{16} = 51(0.008,41)$[15,16] with the condition-limiting reflections hkl: $h + k + l = 2n$, leading to the extinction symbol I − − −. The samples were always contaminated by small amounts of $K_2SrTa_2O_7$ or by an unknown phase, which was indexed by TREOR with an orthorhombic cell (space group: *Pbcn*, $a = 8.381$ Å, $b = 9.763$ Å, $c = 7.853$ Å). The refinement was then performed with a two phase option: $K_2Sr_{1.5}Ta_3O_{10}$ and the orthorhombic impurity which was handled by the Le Bail method.[17]

Background correction was made manually. In the angular range 2θ 10–130°, a total of 169 'F_{obs}' amplitude factors were extracted for the anhydrous form by the Le Bail method[17] by iterating the Rietveld[12] decomposition formula in the space group *I*4/*mmm*.

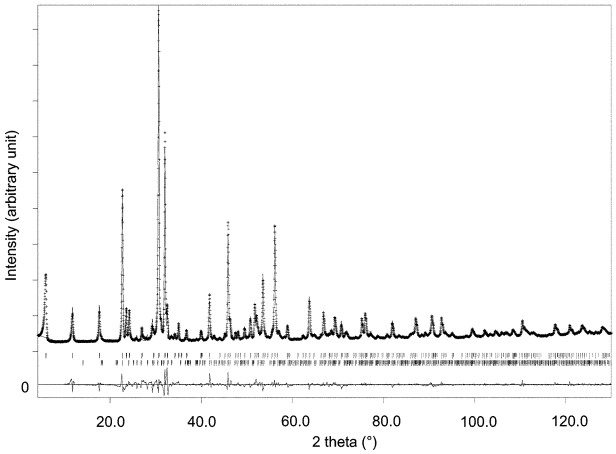

Fig. 1 Observed (···) and calculated (—) powder X-ray diffraction patterns for $K_2Sr_{1.5}Ta_3O_{10}$ at 200 °C in the *I*4/*mmm* space group (no. 139). The difference pattern is shown below at the same scale (vertical bars are related to the calculated Bragg reflection positions). Upper tick: $K_2Sr_{1.5}Ta_3O_{10}$ and lower tick: orthorhombic impurity. The first reflection at low 2θ is not included in final refinement, due to its high asymmetry.

The direct methods from the SHELXS-86 program[18] permitted location of the three heavy atom positions. Atomic scattering factors and anomalous dispersion terms were taken from International Tables for X-ray Crystallography.[19]

These positions formed the initial model (Table 2) for the Rietveld refinements using the FULLPROF program.[13] Oxygen sites are located after subsequent cycles of refinement and difference Fourier synthesis with the program SHELXL-93.[20] The structure was found to be similar to that of $K_2CaNaTa_3O_{10}$,[9] Sr partially replacing (Ca, Na) and leading to vacancies. The presence of these vacancies on the 12-coordinated site allowed possible occupation by K^+, an assumption supported by the fact that Sr–O and K–O distances are equivalent. Such a behavior was previously encountered, for instance, in $(Sr,K)_3Bi_2O_7$.[21] Moreover, valence bond calculations[22] were found much better with this model than calculations performed with all potassium atoms located in (0, 0, 0.285). With partial distribution of potassium atoms on

Table 1 Conditions of X-ray data collection and crystallographic characteristics of $K_2Sr_{1.5}Ta_3O_{10}$

Diffractometer	Siemens D501
Radiation	Cu-Kα, graphite diffracted beam monochromator
Settings	38 kV, 28 mA
Receiving slit/°	0.05
Angular range, 2θ/°	4.2–130 acquisition, 10–130 for refinement
Step scan increment, 2θ/°	0.02
Count time/s $step^{-1}$	40
Miscellaneous	200 °C, no sample rotation
Space group	*I*4/*mmm* (no.139)
Cell parameters/Å	$a = 3.9626(1)$, $c = 30.3257(7)$
Volume/Å^3, Z	476.19(1), 2
Number of reflections	169
Number of refined parameters	18
Halfwidth parameters	$U = 0.145(7)$, $V = -0.129(7)$, $W = 0.073(2)$
Peak shape, η	Pseudo-Voigt, 0.76(2)
Zero point, 2θ/°	0.1242(1)
Asymmetry parameters	$P1 = 0.076(9)$, $P2 = 0.011(2)$
Preferred orientation[a]	[110] direction, 0.174(3)
Reliability factors[b]	$R_p = 0.122$, $R_{wp} = 0.148$, $R_{Bragg} = 0.046$, $\chi^2 = 22.5$

[a]See ref. 13. [b]R_p and R_{wp} are conventional Rietveld values, calculated after background subtraction.

Table 2 Atomic coordinates and thermal parameters for $K_2Sr_{1.5}Ta_3O_{10}$ and $K_2Sr_{1.5}Ta_3O_{10}\cdot H_2O$ (standard deviations are given in parentheses)

Atoms	*x*	*y*	*z*	*B*/Å^2	Site	Occupancy
$K_2Sr_{1.5}Ta_3O_{10}$ (at 200 °C)						
K	0	0	0.285(1)	6.5(3)	4e	0.88
Ta1	0	0	0	0.56(2)	2a	
Ta2	0	0	0.13945(5)	0.56(2)	4e	
Sr/K	½	½	0.0704(1)	0.688(3)	4e	0.75/0.12
O1	0	0	0.1975(5)	0.7(1)	4e	
O2	0	½	0.1325(4)	0.7(1)	8g	
O3	0	0	0.0639(6)	0.7(1)	4e	
O4	0	½	0	0.7(1)	4c	
$K_2Sr_{1.5}Ta_3O_{10}\cdot H_2O$						
K	½	½	0.3924(8)	0.80	2h	0.84
Ta1	0	0	0	0.60	1a	
Ta2	0	0	0.2477(3)	0.60	2g	
Sr/K	½	½	0.1247(6)	0.70	2h	0.75/0.16
O1	0	½	0	0.95	2f	
O2	0	0	0.123(3)	0.95	2g	
O3	0	½	0.239(2)	0.95	4i	
O4	0	0	0.366(3)	0.95	2g	
O5(w)	0	0	½	0.95	1b	

the 12-coordinated perovskite cages site, final Rietveld refinement leads to $R_{Bragg} = 0.05$.

Another point should be noted: the isotropic *B* value for K^+ in 4e site is very high which may indicate high mobility of this cation in the structure. For example, similar high *B* values were found for alkali metal sites: 4.9 Å^2 in $NaLaNb_2O_7$ and 5.9 Å^2 in $LiLaNb_2O_7$.[23]

Table 1 gathers the crystallographic characteristics and the refined profile parameters together with the reliability factors for $K_2Sr_{1.5}Ta_3O_{10}$. Atomic coordinates and thermal parameters are reported in Table 2 while selected interatomic distances and angles are listed in Table 3. Bond valence calculations are given in Table 5 (later). The mean metal–oxygen distances are in agreement with the sum of the ionic radii,[24] but as usual for powder structure calculations, one cannot expect a very high precision on the positional parameters of light atoms because of the presence of heavy scatterers.

$K_2Sr_{1.5}Ta_3O_{10}$: structural description

The structure of anhydrous $K_2Sr_{1.5}Ta_3O_{10}$ (Fig. 2) is similar to that of other $n = 3$ layered perovskites such as $K_2La_2Ti_3O_{10}$ [25] and $K_2CaNaTa_3O_{10}$.[9] It consists of triple-layer perovskite slabs interleaved with potassium ions in a rocksalt-type layer. Two successive layers are shifted by $(a + b)/2$. The large Sr cations

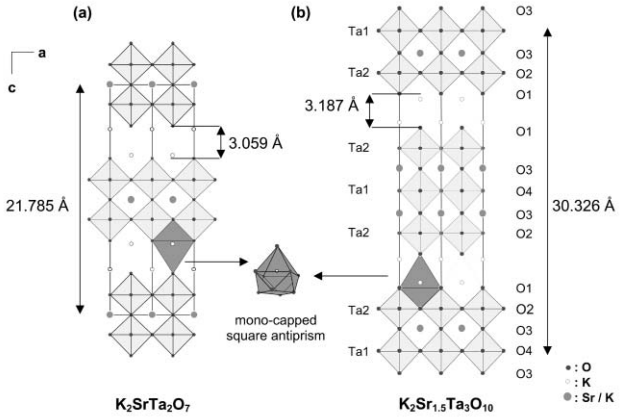

Fig. 2 Projection of the crystal structure of $K_2SrTa_2O_7$ (a) and $K_2Sr_{1.5}Ta_3O_{10}$ (b) showing the perovskite lattice and the potassium coordination polyhedron.

partially occupy the 12-coordinated A sites with 25% of vacancies rate while Ta cations occupy the B sites of perovskite. The potassium atoms are located in a mono-capped square antiprism (C.N. 9, see Fig. 2), coordination already observed in K_2NiF_4.[26] This stacking feature is similar to that observed in $K_2SrTa_2O_7$ and in the series $Li_2A_{0.5n}B_nO_{3n+1}$.[1,2] However, in $MCa_2Ta_3O_{10}$ (M = Li, Na, K, Rb, Cs)[4] the relative arrangement is dependent on the size of ions located in the interlayer spacing: the perovskite layers can be stacked without displacement (cesium and rubidium compounds), with a displacement by ½ along only one direction within the layer plane (potassium compound) or with a displacement by ½ along the diagonal direction within the layer plane (sodium and lithium compounds).

As it is well known in layered perovskites, the TaO_6 octahedra forming the outer layer of the slabs are characterized by off-centering of the Ta atoms, leading to four equal equatorial Ta–O distances within the perovskite layers (1.981 Å), a short Ta–O bond toward the interlayer spacing (1.76 Å) and a long opposite Ta–O bond (2.29 Å). The octahedra forming the middle layer are less distorted with Ta–O distances ranging from 1.94 to 1.98 Å.

Concerning the potassium atom, the coordination polyhedron involves three different K–O bonds ranging from 2.66 to 3.19 Å. The shortest one (2.66 Å) is observed with the terminal oxygen atom O1 of the nearest TaO_6 octahedron. These distances, as for the Sr–O ones (2.733–2.913 Å) are in good agreement with the values in the literature.

Table 3 Selected interatomic distances (Å) and angles (°) for $K_2Sr_{1.5}Ta_3O_{10}$ and $K_2Sr_{1.5}Ta_3O_{10}\cdot H_2O$

Ta1 octahedron	Ta2 octahedron	Sr/K polyhedron	K polyhedron
$K_2Sr_{1.5}Ta_3O_{10}$			
Ta1–O3: 2 × 1.94(2)	Ta2–O1: 1 × 1.76(1)	Sr/K–O2: 4 × 2.733(1)	K–O1: 1 × 2.66(2)
Ta1–O4: 4 × 1.981(0)	Ta2–O2: 4 × 1.992(2)	Sr/K–O3: 4 × 2.809(2)	K–O1: 4 × 2.851(3)
	Ta2–O3: 1 × 2.29(2)	Sr/K–O4: 4 × 2.913(3)	K–O2: 4 × 3.19(1)
O3–Ta1–O3: 180(2)	O1–Ta2–O2: 96.1(8)		
O3–Ta1–O4: 90.0(7)	O1–Ta2–O3: 180(1)		
O4–Ta1–O4: 180.0(1)	O2–Ta2–O2: 167.9(5)		
O4–Ta1–O4: 90.0(1)	O2–Ta2–O2: 89.4(5)		
	O2–Ta2–O3: 83.9(7)		
$K_2Sr_{1.5}Ta_3O_{10}\cdot H_2O$			
Ta1–O1: 4 × 1.975(1)	Ta2–O2: 1 × 2.12(5)	Sr/K–O1: 4 × 2.90(1)	K–O3: 4 × 3.28(3)
Ta1–O2: 2 × 2.10(5)	Ta2–O3: 4 × 1.981(3)	Sr/K–O2: 4 × 2.79(3)	K–O4: 4 × 2.83(3)
	Ta2–O4: 1 × 2.01(5)	Sr/K–O3: 4 × 2.77(3)	K–O5(w): 4 × 3.34(1)
O1–Ta1–O1: 180.0(1)	O2–Ta2–O3: 85(2)		
O1–Ta1–O1: 90.00(1)	O2–Ta2–O4: 180(4)		
O1–Ta1–O2: 90(2)	O3–Ta2–O3: 170.9(1)		
O2–Ta1–O2: 180(4)	O3–Ta2–O3: 89.6(1)		
	O3–Ta2–O4: 94(2)		

The interlayer spacings are nearly independent of n: 3.059 Å for $K_2SrTa_2O_7$ ($n = 2$) compared to 3.187 Å for $K_2Sr_{1.5}Ta_3O_{10}$ ($n = 3$). However, such values can be correlated to the relative charge density of the perovskite layer which is the same in the two considered members.

At this stage of this study, this transformation leads us to make several remarks: (i) such a transformation leading to a new tantalum RP phase is probably a topotactic one since the layered structure is preserved. (ii) The two forms $n = 2$ and $n = 3$ coexist if the annealing temperature is too low probably due to a slow kinetic process. (iii) Surprisingly, we observe the formation of an $n = 3$ member while one can imagine that the formation of an $n = 4$ member, implying only a condensation and a sliding of two successive perovskite blocks, seems easier. Indeed, the passage of $n = 2$ towards $n = 3$ needs first a scission of some of the Ta–O bonds, followed by a sliding of the perovskite slabs and finally a condensation of the slabs. During this transformation, a third of the K^+ ions present in the mother-phase is lost and a migration of K^+ and Sr^{2+} ions is observed: the refinement of the $n = 3$ member shows that about 12% of the K^+ ions are located in the 12-coordinated perovskite sites, probably trapped during the structural reorganization. Most of the RP phases have an ordered structure contrarily with the observation of Vallino[27] who claimed that the distribution of alkali metal and lanthanum ions in $M_2La_2Ti_3O_{10}$ (M = Li, Na, K) is disordered. In $K_2Sr_{1.5}Ta_3O_{10}$, a disordered distribution of K^+ ions is found implying vacancy distribution over the two 12- and 9-coordinated sites, a situation which is very promising for ionic conductivity measurements. As already mentioned, it should be pointed out that such a transformation is probably facilitated by similar Sr–O and K–O distances, which allows exchange of the two cations over the two sites. It would be very interesting to investigate the same transformation with other RP phases containing very different A, A′ cations: as mentioned above, our tests to prepare $Li_2Sr_{1.5}Ta_3O_{10}$ from $Li_2SrTa_2O_7$ were unsuccessful.

$K_2Sr_{1.5}Ta_3O_{10}$: water intercalation

As for many layered perovskites,[9,10,28] the two-dimensional structure of $K_2Sr_{1.5}Ta_3O_{10}$ allows spontaneous water intercalation when exposed to air under ambient condition. This behavior was already observed for the $n = 2$ parent compound $K_2SrTa_2O_7$ for which a slow hydration and no saturation in water insertion (even after one month) were observed.[29] For this phase, the number of water molecules per formula unit was only dependant on the humidity of the atmosphere, a result in disagreement with that proposed by Kodenkandatt and Wiley[10] who claimed that a plateau of water intake was obtained.

Concerning water intercalation in RP phases, it is interesting that, as already noticed,[25] the lithium compound does not exist in any hydrated form, even when the compound is washed with distilled water. This difference can probably be explained by a smaller interlayer space in the Li compound, which does not allow the water insertion.

$K_2Sr_{1.5}Ta_3O_{10}\cdot H_2O$: structural determination

As mentioned above, the X-ray pattern of the hydrated form was recorded at room temperature (Fig. 3a) after sample exposure to ambient air for several hours. The procedure for the structure determination was the same as the one used for the anhydrous form $K_2Sr_{1.5}Ta_3O_{10}$: auto-indexing was performed by using the TREOR[13] program applied to the first 12 detected lines for $K_2Sr_{1.5}Ta_3O_{10}\cdot H_2O$. A tetragonal space group was found and characterized by the conventional figures of merit $M_{12} = 77$ and $F_{12} = 45$, with no condition-limiting

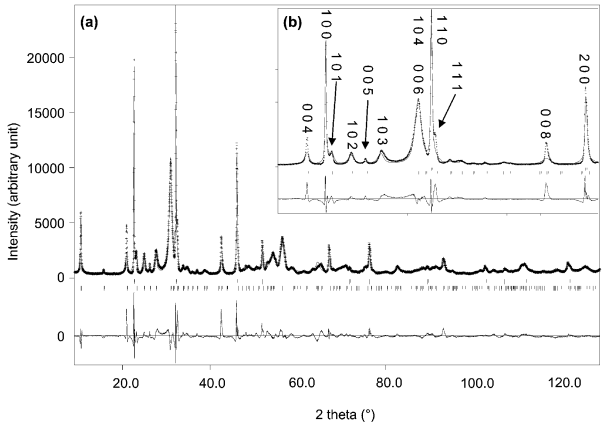

Fig. 3 Observed (···), calculated (—) and difference powder X-ray diffraction patterns for $K_2Sr_{1.5}Ta_3O_{10}\cdot H_2O$ (a) at room temperature in the *P4/mmm* space group (no. 123) (vertical bars are related to the calculated Bragg reflection positions). Upper tick: (*hk*0) reflections and lower tick: (*hkl*) reflections. A small part of the X-ray powder diffraction pattern showing broad (*hkl*) and sharp (*hk0*) reflections is zoomed in (b).

reflections giving the possible space group *P4/mmm* (no.123) ($a = 3.9499(2)$ Å and $c = 17.031(3)$ Å).

X-Ray reflections in $K_2Sr_{1.5}Ta_3O_{10}\cdot H_2O$ exhibit a very large anisotropic behavior: reflections (*hkl*) are relatively broad whereas reflections (*hk*0) are very sharp (Fig. 3b). The latter type of reflections cannot definitively be handled by a Pseudo-Voigt function. In our case, only the Pearson VII function is able to fit approximately the (*hk*0) peaks, explaining the very high R_p and R_{wp} values. This feature is probably due to the poor crystallinity of the sample together with a stacking disorder of perovskite slabs.

Table 4 gathers the crystallographic characteristics and the final refined profile while atomic coordinates and thermal parameters are given in Table 2. Fourier synthesis allowed to clear location of the water molecule in the 1b site of the

Table 4 Conditions of X-ray data collection and crystallographic characteristics of $K_2Sr_{1.5}Ta_3O_{10}\cdot H_2O$

Diffractometer	Bruker D8
Radiation	Cu-Kα, graphite diffracted beam monochromator
Settings	40 kV, 40 mA
Divergence, antiscattering slits/°	0.5, 0.5
Receiving slit/°	0.2
Angular range, 2θ/°	9–129 for refinement
Step scan increment, 2θ/°	0.02
Count time/s step^{-1}	53
Miscellaneous	Room temperature, no sample rotation
Space group	*P4/mmm* (no.123)
Cell parameters/Å	$a = 3.9499(2)$, $c = 17.031(3)$
Volume/Å^3, Z	265.71(6), 1
Number of reflections	188 (*hk*0 = 12, *hkl* = 176)
Number of refined parameters	22
Halfwidth parameters (*hk*0)	$U = 0.03(1)$, $V = -0.004(10)$, $W = 0.019(2)$
Peak shape, M	Pearson VII, 1.07(2)
Halfwidth parameters (*hkl*)	$U = -0.8(1)$, $V = -2.6(1)$, $W = -0.12(2)$
Peak shape, η	Pseudo-Voigt, 0.84(5)
Zero point, 2θ/°	0.196(3)
Asymmetry parameters	$P1 = 0.090(4)$, $P2 = -0.008(2)$
Preferred orientation	[*0 0 1*] direction, 0.110(4)
Reliability factors[a]	$R_p = 0.26$, $R_{wp} = 0.30$, $\chi^2 = 32.6$ R_{Bragg} (*h k 0*) = 0.07, R_{Bragg} (*h k l*) = 0.11

[a] R_p and R_{wp} are conventional Rietveld values, calculated after background subtraction.

Table 5 Valence bond analysis for $K_2Sr_{1.5}Ta_3O_{10}$ and $K_2Sr_{1.5}Ta_3O_{10}\cdot H_2O$ using the Zachariasen law.[22a]

Atom	O1	O2	O3	O4	O5(w)	Σ	$\Sigma_{expected}$
$K_2Sr_{1.5}Ta_3O_{10}$							
Ta1			2 × 0.95	4 × 0.85		5.30	5
Ta2	1.54	4 × 0.82	0.37			5.19	5
K	0.24 + 4 × 0.14	4 × 0.06				1.04	1
Sr		4 × 0.19	4 × 0.15	4 × 0.12		1.84	2
Σ	2.34	2.26	1.91	2.12			
Σexpected	2	2	2	2			
$K_2Sr_{1.5}Ta_3O_{10}\cdot H_2O$							
Ta1	4 × 0.86	2 × 0.62				4.68	5
Ta2		0.58	4 × 0.85	0.78		4.76	5
K			4 × 0.05	4 × 0.15	4 × 0.04	0.96	1
Sr	4 × 0.12	4 × 0.16	4 × 0.17			1.80	2
Σ	2.20	1.84	2.14	1.37	0.32		
Σexpected	2	2	2	2	2		

[a] $s = \exp[(R_0 - R)/B]$; $B = 0.37$, $R_0 = 1.920$, 2.118 and 2.130, respectively, for Ta, Sr, K.

P4/mmm space group (0 0 ½), position that differs from that given for $K_2Ca_2Ta_2TiO_{10}\cdot 0.8H_2O$.[9] Interatomic distances and bond valence calculations are given in Tables 3 and 5, respectively. The absence of a valency value for both O4 and O5 can be explained easily: the hydrogen atoms were not located in this structure and these atoms provided the complement of the missing valence (hydrogen bonds with O4 and covalent bonds with O5).[30,31]

$K_2Sr_{1.5}Ta_3O_{10}\cdot H_2O$: structural description

As often observed in layered perovskites,[4,28,32] the hydration process generates a structural transformation resulting from an $(a + b)/2$ shift of the central slab relative to the adjacent one. This transition from a body centered to primitive lattice leads to a halving of the *c*-axis length ($c = 30.3257(7)$ to 17.031(3) Å). Consequently, the different atoms remain in the same environment except for the potassium which is now surrounded by 12 oxygen atoms (CN = 9 in $K_2Sr_{1.5}Ta_3O_{10}$). This resultant polyhedron (Fig. 4) involves three different K–O bonds (4 × K–O3, 4 × K–O4 and 4 × K–O5(w)). Concerning the perovskite layer, we observe the same configuration as in the anhydrous form: the TaO_6 octahedra located on the inside layers ($Ta1O_6$) are less distorted than those located on the outside of the layer ($Ta2O_6$). The $Ta1O_6$ octahedra are characterized by two types of distances (1.975 and 2.10 Å), while the $Ta2O_6$ octahedra show three types of distances: four equal equatorial bonds (1.981 Å), a long bond with the O2 atom which belongs to the next octahedron of the same slab (2.12 Å) and a shorter one (2.01 Å) in the direction of the interlayer alkali metal. These values show that under hydration the $Ta2O_6$ octahedron becomes more regular connected to the evolution of the Ta2–O bonds along the *c*-axis.

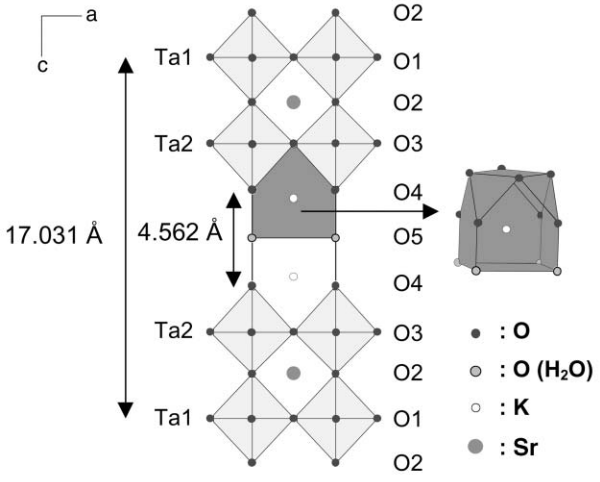

Fig. 4 Crystal structure of $K_2Sr_{1.5}Ta_3O_{10}\cdot H_2O$ viewed along the *c*-axis.

$K_2Sr_{1.5}Ta_3O_{10}\cdot H_2O$: thermal analysis

The capacity of absorption/desorption of water was studied by DTA/TGA measurements performed on one cycle of dehydration–hydration (Fig. 5). The compound was first heated at 200 °C under an argon flow for 2 h (Fig. 5a) in order to enable the departure of water ($\Delta m/m = -2.3\%$). Then the sample was cooled (T_{room}) under an air flow saturated with water during 15 h. During this step and as we can see in Fig. 5b, the sample weight increases until a saturation level is reached. This mass gain (+2.4%) corresponds to the loss observed during the

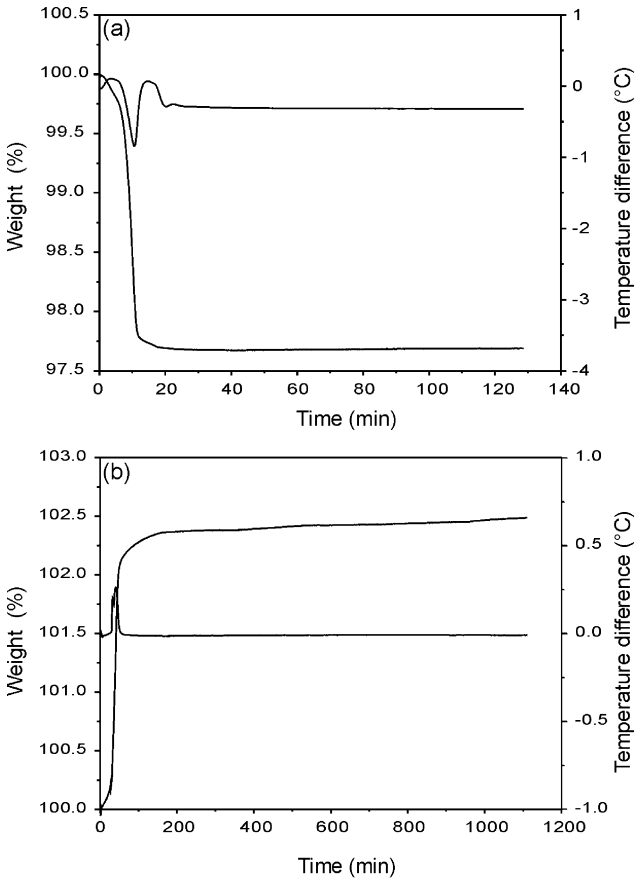

Fig. 5 DTA and TGA curves showing the dehydration (a) and hydration (b) process for $K_2Sr_{1.5}Ta_3O_{10}\cdot H_2O$.

heating, meaning that the water intercalation is reversible and leads to a stable hydrate. On the DTA curve, we observe that the weight variation is always connected to a peak. Assuming the compound is anhydrous after the heating, the weight variation (2.3%) corresponds to the loss or to the absorption of 1.1 ± 0.1 water molecules per unit cell leading to the formulation $K_2Sr_{1.5}Ta_3O_{10}\cdot H_2O$ which is in agreement with the structural study. Compared to $K_2SrTa_2O_7$, the structural transition (I to P lattice) due to water intercalation proceeds more quickly preventing this phenomenon being followed by X-ray diffractometry, the coexistence time of the anhydrous and hydrated forms being too short.

$K_2Sr_{1.5}Ta_3O_{10}$: proton exchange

K^+/H^+ exchange was carried out in acid solution (100 ml of 2 M HNO_3) on 0.5 g of anhydrous $K_2Sr_{1.5}Ta_3O_{10}$, the solution being maintained at around 60 °C for one day under constant stirring. The solid was then filtered off, washed with distilled water and air dried. K content analysis of the filtrate, performed using flame photometry, showed that the ionic exchange was incomplete (80%) leading to the formulation $H_{1.60}K_{0.40}Sr_{1.5}Ta_3O_{10}$. Then, we tried to optimize the exchange by changing the operating conditions (HNO_3 concentration, time of exchange, temperature, consecutive exchanges···) but unfortunately, it was impossible to improve the result, meaning that some of the potassium is probably inaccessible to ion exchange. Such a situation can be explained both by the presence of the unknown impurity in all our samples and by the probable localization of a part of the potassium on the dodecahedral sites which presents 25% of vacancies. This explanation has already been proposed by Fang *et al.*[33] in the case of the layered perovskite $KCa_2Nb_3O_{10}$. The poor crystallinity of the samples prevents us from solving the crystal structure of the exchanged phase.

Conclusion

During this work, $K_2Sr_{1.5}Ta_3O_{10}$ and its monohydrate have been structurally characterized by X-ray powder diffraction. Their structures are strongly related to those found for the $n = 3$ member layered perovskite Ruddlesden–Popper phases and are built from three thick TaO_6 octahedra perovskite slabs. Most of the K^+ ions are located in the interlayer with the remainder being distributed with all Sr^{2+} ions and vacancies in the A sites of the perovskite blocks. We have described, for the first time in this type of compounds, the formation of an $n = 3$ member from an $n = 2$ member by a controlled thermal decomposition process, illustrating the low cohesion of the structure owing to the loose K–O bonding in the interlayer. This situation is different from that found in the lithium homolog where the Li–O bonding is stronger, explaining probably why such a transformation from $n = 2$ to $n = 3$ is not observed for $Li_2SrTa_2O_7$. The loose K–O bonding is also related to the fast and reversible hydration process observed for $K_2Sr_{1.5}Ta_3O_{10}$, leading to a new monohydrate $K_2Sr_{1.5}Ta_3O_{10}\cdot H_2O$; this process, also encountered for the $n = 2$ member, is classically associated to the topotactic transformation leading to the I ↔ P lattice structural change.

References

1 N. S. P. Bhuvanesh, M. P. Crosnier-Lopez, O. Bohnke, J. Emery and J. L. Fourquet, *Chem. Mater.*, 1999, **11**, 634.
2 N. S. P. Bhuvanesh, M. P. Crosnier-Lopez and J. L. Fourquet, *J. Mater. Chem.*, 1999, **9**, 3093.
3 (*a*) A. J. Jacobson, J. T. Lewandowski and J. W. Johnson, *J. Less-Common Met.*, 1984, **21**, 92; (*b*) A. J. Jacobson, J. W. Johnson and J. T. Lewandowski, *Mater. Res. Bull.*, 1987, **22**, 45; (*c*) J. Gopalakrishnan and V. Bhat, *Inorg. Chem.*, 1987, **26**, 4299.
4 K. Toda, T. Teranishi, Z. G. Ye, M. Sato and Y. Hinatsu, *Mater. Res. Bull.*, 1999, **34**, 971.
5 V. Thangadurai, P. Schmid-Beurmann and W. Weppener, *J. Solid State. Chem.*, 2001, **158**, 279.
6 K. Toda, T. Suzuki and M. Sato, *Solid State Ionics*, 1997, **93**, 177.
7 N. S. P. Bhuvanesh, M. P. Crosnier-Lopez, H. Duroy and J. L. Fourquet, *J. Mater. Chem.*, 2000, **10**, 1685.
8 P. J. Ollivier and T. E. Mallouk, *Chem. Mater.*, 1998, **10**, 2585.
9 R. E. Schaak and T. E. Mallouk, *J. Solid State Chem.*, 2000, **155**, 46.
10 T. H. Kodenkandath and J. B. Wiley, *Mater. Res. Bull.*, 2000, **35**, 1737.
11 M. Sato, J. Abo, T. Jin and M. Ohta, *Solid State Ionics*, 1992, **51**, 89.
12 H. M. Rietveld, *J. Appl. Crystallogr.*, 1969, **2**, 65.
13 J. Rodriguez-Carvajal, Program FULLPROF, version 3.5, 1998.
14 P. E. Werner, L. Erikson and M. Westdhal, *J. Appl. Crystallogr.*, 1985, **18**, 367.
15 P. M. D. Wolff, *J. Appl. Crystallogr.*, 1968, **1**, 108.
16 G. S. Smith and R. L. Snyder, *J. Appl. Crystallogr.*, 1979, **12**, 60.
17 A. Le Bail, *NIST Special Publ.*, 1992, **846**, 213.
18 G. M. Sheldrick, *SHELXS-86, in Crystallographic Computing 3*, ed. G. M. Sheldrick, C. Krüger and R. Goddard, Oxford University Press, 1985.
19 *International Tables for X-ray Crystallography*, Kluwer, Dordrecht, 1992, vol.C.
20 G. M. Sheldrick, SHELXL-93: A program for the refinement of crystal structures from diffraction data, University of Göttingen, 1993.
21 J. S. Pshirkov, S. M. Kazakov, C. Bougerol-Chaillout, P. Bordet, J. J. Capponi, S. N. Putilin and E. V. Antipov, *J. Solid State Chem.*, 1999, **144**, 405.
22 N. E. Brese and O. Keefe, *Acta Crystallogr., Sect B*, 1991, **47**, 192.
23 M. Sato, J. Abo, T. Jin and M. Ohta, *J. Alloys Compd.,*, 1993, **192**, 81.
24 R. D. Shannon, *Acta Crystallogr., Sect. A*, 1976, **32**, 751.
25 K. Toda, J. Watanabe and M. Sato, *Mater. Res. Bull.*, 1996, **31**, 1427.
26 D. Babel and A. Tressaud, *Inorganic Solid Fluorides*, ed. P. Hagenmuller, Academic Press, Inc., New York, London, 1985.
27 M. Vallino, *Atti Accad. Sci. Torino. Cl., Sci. Fis. Mat. Nat.*, 1983, **117**, 85.
28 M. Richard, L. Brohan and M. Tournoux, *J. Solid State Chem.*, 1994, **112**, 345.
29 M. P. Crosnier-Lopez, F. Le Berre and J. L. Fourquet, *J. Mater. Chem.*, 2001, **11**, 1146.
30 M. P. Crosnier-Lopez and J. L. Fourquet, *J. Solid State Chem.*, 1993, **105**, 92.
31 A. Hémon-Ribaud, M. P. Crosnier-Lopez, J. L. Fourquet and G. Courbion, *J. Fluorine Chem.*, 1994, **68**, 155.
32 Y. S. Hong, C. H. Han and K. Kim, *J. Solid State Chem.*, 2001, **158**, 290.
33 M. Fang, C. H. Kim and T. E. Mallouk, *Chem. Mater.*, 1999, **11**, 1519.